JACS
JOURNAL OF THE AMERICAN CHEMICAL SOCIETY

COMMUNICATION

pubs.acs.org/JACS

Electron Transfer Cascade by Organic/Inorganic Ternary Composites of Porphyrin, Zinc Oxide Nanoparticles, and Reduced Graphene Oxide on a Tin Oxide Electrode that Exhibits Efficient Photocurrent Generation

Hironobu Hayashi,[†] Ian V. Lightcap,[‡] Masahiko Tsujimoto,[§] Mikio Takano,[§] Tomokazu Umeyama,[†] Prashant V. Kamat,[*,‡] and Hiroshi Imahori[*,†,§]

[†]Department of Molecular Engineering, Graduate School of Engineering, Kyoto University, Nishikyo-ku, Kyoto 615-8510, Japan

[‡]Radiation Laboratory, Department of Chemistry and Biochemistry, University of Notre Dame, Notre Dame, Indiana 46556, United States

[§]Institute for Integrated Cell-Material Sciences (iCeMS), Kyoto University, Nishikyo-ku, Kyoto 615-8510, Japan

Supporting Information

ABSTRACT: A bottom-up strategy has been developed to construct a multiple electron transfer system composed of organic/inorganic ternary composites (porphyrin, zinc oxide nanoparticles, reduced graphene oxide) on a semiconducting electrode without impairing the respective donor−acceptor components. The hierarchical electron transfer cascade system exhibited remarkably high photocurrent generation with an incident-photon-to-current efficiency of up to ca. 70%.

Core to photosynthesis is the multistep electron transfer (ET) of supramolecularly assembled photofunctional chromophores in protein.[1] Such well-organized multistep ET systems allow photosynthesis to achieve efficient solar energy conversion. To mimic the multistep ET, various attempts have been made in artificial systems.[2] However, it is still a challenge to organize suitable organic/inorganic materials in a bottom-up manner, forming a hierarchical ET cascade on an electrode without impairing the intrinsic structures and functions. Here, we report an approach to construct a multistep ET system exhibiting efficient photocurrent generation. It utilizes porphyrin (ZnP, Figure 1),[3] zinc oxide nanoparticles (ZnONP's), and reduced graphene oxide (RGO) as donor−acceptor components. They are sequentially organized on an electrode, that is, by (i) anchoring of the ZnONP's on RGO as a two-dimensional (2D) scaffold, (ii) adsorption of ZnP on the ZnONP's on RGO, and (iii) electrophoretic deposition of the resulting organic/inorganic composites onto sintered SnO_2 nanoparticles on an FTO electrode (denoted as FTO/SnO_2) (Figure 1).

An FTO/SnO_2 electrode was modified with ZnP, ZnONP, and RGO composites as follows. First, graphene oxide (GO) was prepared by the treatment of graphite powder with a strong acid, followed by filtration.[4] This oxidation process introduces hydroxyl and epoxy groups into the graphene sheet, along with carbonyl and carboxyl groups into the edges.[5] The dried product was suspended in ethanol and mildly sonicated to disperse the

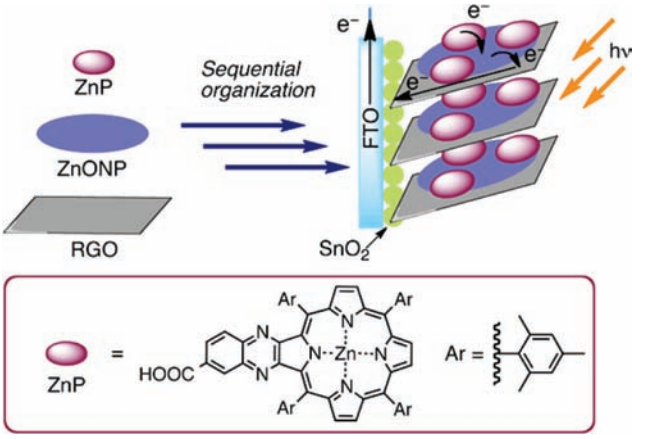

Figure 1. Hierarchical electron cascade system on an electrode.

GO sheets. Figure S1A displays an atomic force microscopy (AFM) image of GO after the sonication process. The graphene sheets exist as fragments with an average area of 0.38 μm^2 owing to the oxidation process (Figure S1B). The average thickness of the GO sheet was determined as ca. 1.0 nm, which is consistent with that of fully exfoliated GO sheets[6] (Figure S1C).

The next step is the anchoring of the ZnONP's onto RGO. Initially, ZnONP's were suspended in ethanol.[7] Then, an ethanol suspension of ZnONP's with GO was mildly sonicated under N_2 saturated conditions to coat the ZnONP's on GO. UV-irradiation of GO−ZnONP has been previously shown to result in the photocatalytic reduction of GO.[8] During the process, the suspension changed color from pale brown to pale black (Figure S2). This is rationalized by considerable restoration of the conjugated π network in graphene sheets via photoreduction by the excited ZnONP's anchored on the graphene sheet. *n*-Heptane was added to the suspension so that RGO−ZnONP composites were precipitated from the solution. Transmission electron microscopy (TEM) measurement was performed to evaluate the surface

Received: February 28, 2011
Published: April 26, 2011

dx.doi.org/10.1021/ja201813n | *J. Am. Chem. Soc.* 2011, 133, 7684–7687

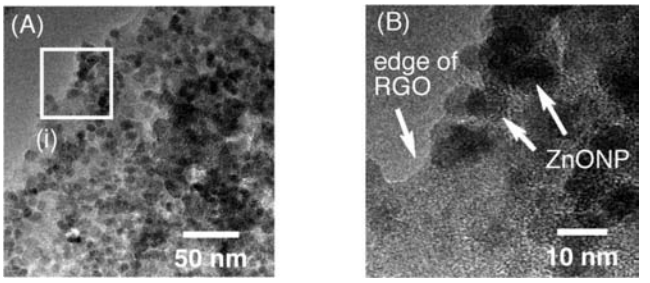

Figure 2. TEM images of ZnONP−RGO composite. The enlarged image of area (i) is shown as (B). A dilute sample was drop-cast on a carbon grid for the measurement.

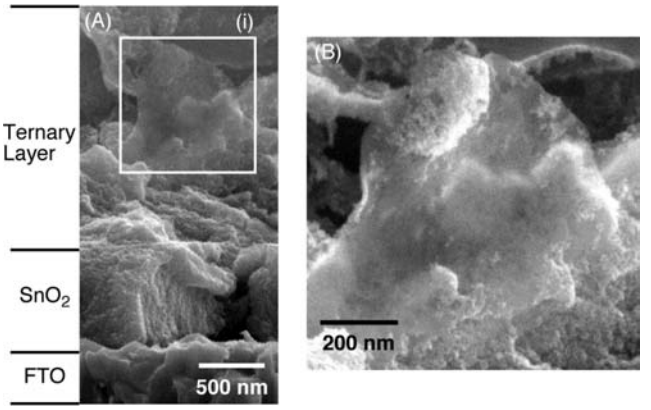

Figure 3. (A) Cross-sectional FE-SEM images of the FTO/SnO_2/$(RGO-ZnONP-ZnP)_m$ electrode. The enlarged image of area (i) is shown as panel (B).

morphology. A typical TEM image of ZnONP's anchored onto the RGO sheets is given in Figure 2. Both ZnONP's and the edge of RGO are evident. The ZnONP observed in the TEM image has a small spherical structure with a size of ca. 7 nm.[7] It is noteworthy that the RGO sheets are densely covered by ZnONP's. Such oxide nanoparticles anchored on the surfaces of RGO are favorable to prevent the exfoliated RGO sheets from direct stacking after photoreduction of the GO.[8]

Finally, the RGO−ZnONP composites were stirred in a 0.2 mM ZnP methanol solution to adsorb ZnP molecules onto the RGO−ZnONP composites. The resulting composites were centrifuged and subsequently washed with methanol. To a toluene suspension of the composites, acetonitrile was injected rapidly, resulting in formation of the ternary composites $(RGO+ZnONP+ZnP)_m$ in the mixed solvents. The ternary composites were electrophoretically deposited onto an FTO/SnO_2 electrode (denoted as FTO/SnO_2/$(RGO+ZnONP+ZnP)_m$).[2e] The absorption spectrum of the FTO/SnO_2/$(RGO+ZnONP+ZnP)_m$ electrode shows the Soret and Q bands of ZnP, implying that ZnP molecules adsorb onto the composite film (Figure S3). Moreover, the FE-SEM and TEM measurements also reveal that the RGO sheets on the electrode are wrapped with ZnO nanoparticles that are further coated with ZnP molecules (Figure S4). These results suggest that the RGO sheets serve as a 2D network, which would be able to facilitate electron flow from the ZnONP−ZnP composites to the FTO/SnO_2 electrode (vide infra). To further examine the morphology of the FTO/SnO_2/$(RGO+ZnONP+ZnP)_m$

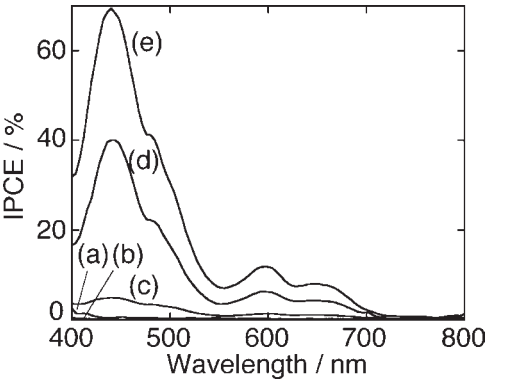

Figure 4. Photocurrent action spectra of the (a) FTO/SnO_2/$(ZnONP)_m$, (b) FTO/SnO_2/$(RGO+ZnONP)_m$, (c) FTO/SnO_2/$(ZnP)_m$, (d) FTO/SnO_2/$(ZnONP+ZnP)_m$, and (e) FTO/SnO_2/$(RGO+ZnONP+ZnP)_m$ electrodes. Applied potential: 0.05 V vs SCE; 0.5 M LiI and 0.01 M I_2 in acetonitrile as an electrolyte. IPCE values were calculated by normalizing the photocurrent densities for incident light energy and intensity and by use of the expression: IPCE (%) = $100 \times 1240 \times i/(W_{in} \times \lambda)$ = (light harvesting efficiency) × (electron injection efficiency) × (electron collection efficiency), where i is the photocurrent density (A cm^{-2}), W_{in} is the incident light intensity (W cm^{-2}), and λ is the excitation wavelength (nm).

Scheme 1. Schematic Illustration for the Energy Diagram

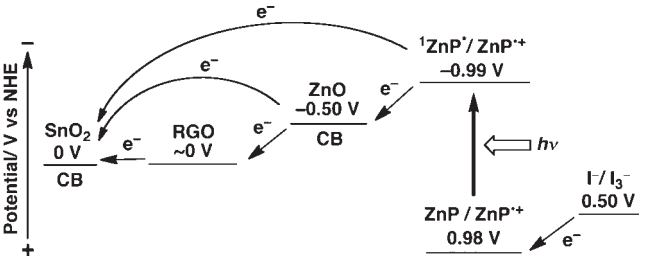

electrode, cross-sectional FE-SEM measurement was employed. It is evident that the $(RGO+ZnONP+ZnP)_m$ composites are firmly deposited on the FTO/SnO_2 electrode (Figure 3). More importantly, we found that the RGO sheets covered by the ZnONP−ZnP composites facilitate electron transport within the composite film. The RGO sheets are randomly distributed in the composite film, and this random network can still facilitate ET to the electrode after collecting electrons in the RGO sheets.[9] These results corroborate an electron-transport pathway to the FTO/SnO_2 electrode through the 2D RGO sheets incorporated during the electrophoretic deposition method. This strategy is analogous to a one-dimensional (1D) fullerene−carbon nanotube (CNT) composite system employed in an earlier study.[10]

To demonstrate the effects of the ET cascade on the photocurrent generation efficiency, we compared the incident photon-to-current efficiency (IPCE) of the photoelectrochemical devices. Figure 4 depicts the photocurrent action spectra for the modified electrodes. The action spectra closely resemble the corresponding absorption spectra of the electrodes (Figure S3). The IPCE value of the FTO/SnO_2/$(ZnP)_m$ device is considerably larger than that of the FTO/SnO_2/$(ZnONP)_m$ and FTO/SnO_2/$(RGO+ZnONP)_m$ electrodes. This implies that direct electron injection from the porphyrin excited singlet state (^{1}ZnP*) to a conduction band (CB) of the SnO_2 electrode has a significant impact on the photocurrent generation (Scheme 1) as established previously.[2d,11]

dx.doi.org/10.1021/ja201813n |J. Am. Chem. Soc. 2011, 133, 7684–7687

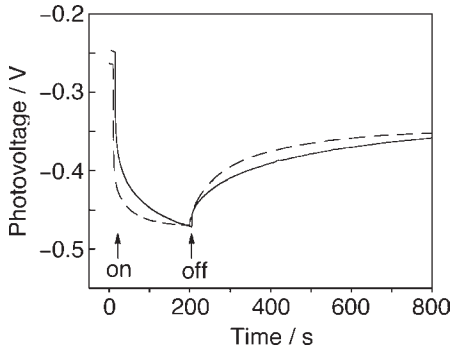

Figure 5. Photovoltage response of the FTO/SnO_2/(RGO+ZnONP+ZnP)$_m$ (solid line) and FTO/SnO_2/(ZnONP+ZnP)$_m$ (dashed line) electrodes under white light illumination (input power: 37.4 mW cm^{-2}, $\lambda > 380$ nm) in a deaerated acetonitrile solution containing 0.1 M TBAP.

The IPCE value of the FTO/SnO_2/(ZnONP+ZnP)$_m$ electrode is enhanced remarkably compared with the FTO/SnO_2/(ZnP)$_m$ electrode. This improvement can be explained by the large contribution to the photocurrent from an additional pathway that electron injection occurs from the ^{1}ZnP* to the CB of the SnO_2 via ZnONP's. More importantly, the IPCE value of the FTO/SnO_2/(RGO+ZnONP+ZnP)$_m$ electrode is further enhanced relative to the FTO/SnO_2/(ZnONP+ZnP)$_m$ electrode. This result unambiguously exemplifies that electron injection takes place from the ^{1}ZnP* to the CB of the SnO_2 via ZnONP and/or RGO, improving the photocurrent generation. It should be emphasized that the maximum IPCE value of the FTO/SnO_2/(RGO+ZnONP+ZnP)$_m$ electrode reaches ca. 70% at 440 nm under an applied potential of 0.05 V vs SCE. Considering that the adsorbed amounts of the ZnP molecules on the composites (6.0×10^{-8} mol cm^{-2}) are comparable for the FTO/SnO_2/(RGO+ZnONP+ZnP)$_m$ and FTO/SnO_2/(ZnONP+ZnP)$_m$ electrodes, we can safely conclude that the improvement results from the difference in the electron injection efficiency and/or electron collection efficiency due to the presence of the RGO and the better configuration for the photocurrent generation. These results imply that the hierarchical ET cascade system is responsible for the occurrence of multistep ET on the electrode, leading to efficient photocurrent generation through the ZnONP and RGO sheets in the device.

To shed light on the effect of the RGO on the photocurrent generation, we conducted photovoltage measurements by monitoring the cell potential response to on−off cycles of visible light illumination. Band gap excitation of ZnONP's using UV-irradiation was used solely for the reduction of GO in the initial ZnONP−GO suspension. Photoelectrochemical characterization was carried out using visible light irradiation thus avoiding any direct excitation of ZnONP's. Under open circuit conditions, the electrons are accumulated in the film by irradiation and then equilibrated with a redox couple (I^-/I_3^-) in the electrolyte. Additionally, the charges in the device are retained within the film for a longer time in a deaerated solution. The rise in potential following the irradiation is observed in the FTO/SnO_2/(RGO+ZnONP+ZnP)$_m$ and FTO/SnO_2/(ZnONP+ZnP)$_m$ electrodes in an acetonitrile solution containing 0.1 M *n*-tetrabutylammonium perchlorate (TBAP) as an electrolyte (Figure 5). In a previously reported CNT−TiO_2 composite system, the magnitude of the photovoltage of the FTO/CNT/TiO_2 electrode is lower than that of the FTO/TiO_2 electrode.[12] This reflects electron transport from TiO_2 to CNT, resulting in the lowering of the Fermi level of the FTO/CNT/TiO_2 electrode. The photovoltage is similar in the FTO/SnO_2/(RGO+ZnONP+ZnP)$_m$ and FTO/SnO_2/(ZnONP+ZnP)$_m$ electrodes as the Fermi level of the working electrode is mainly dictated by the SnO_2 film. The slow rise of photovoltage of the FTO/SnO_2/(RGO+ZnONP+ZnP)$_m$ electrode is indicative of the fact that additional time required electron equilibration in the ZnONP−RGO composite. In addition, the photovoltage decay of the FTO/SnO_2/(RGO+ZnONP+ZnP)$_m$ electrode recorded upon stopping the illumination is slower than that of the FTO/SnO_2/(ZnONP+ZnP)$_m$ electrode. The photovoltage decay directly reflects the longer lifetime of accumulated electrons into the electrolyte. Since, RGO can be regarded as an electron storage material[12] similar to that of CNT,[12a] we expect charge recombination at the electrolyte interface to be less favored.[9,14] Given that the CB of SnO_2 is 0 V vs NHE and the Fermi level of RGO is ∼0 V vs NHE,[15] the difference in the photovoltage decay rate is expected to be small. The presence of RGO influences the overall performance by (i) accepting electrons from the ZnONP−ZnP composites and (ii) providing a medium to store and shuttle electrons within the composite film,[13] as seen in the CNT−TiO_2 composite system.[12] These results also support the occurrence of a multistep ET cascade on the electrode.

On the basis of the film structures and the photoelectrochemical properties of the FTO/SnO_2/(RGO+ZnONP+ZnP)$_m$ systems together with the previously established photocurrent generation mechanism in analogous porphyrin-semiconducting oxide composites,[2e,11] we can propose a photocurrent generation diagram as illustrated in Scheme 1. First, electron injection from ^{1}ZnP* into the CB of ZnONP's (−0.5 V vs NHE)[16] takes place,[17] in addition to minor electron injection from ^{1}ZnP* to the Fermi level of RGO (∼0 V vs NHE)[15] and/or the CB of SnO_2 (0 V vs NHE).[2e,11] In the former case, the collected electrons in the CB of ZnONP's are transferred into the CB of SnO_2 through the 2D RGO network in the ZnONP−ZnP composites, together with electron injection from ZnONP's to the CB of SnO_2. Then, the oxidized porphyrin ($ZnP/ZnP^{+\bullet}$ = 0.98 V vs NHE)[3] undergoes ET reduction with the iodide (I^-/I_3^- = 0.5 V vs NHE)[2e,11] in the electrolyte solution, resulting in the photocurrent generation. Thus, the hierarchical ET cascade system for the FTO/SnO_2/(RGO+ZnONP+ZnP)$_m$ system is responsible for the high photocurrent generation.

In conclusion, we have successfully developed a promising strategy for constructing the efficient hierarchical ET cascade system on a semiconducting electrode in a bottom-up manner by using RGO as a 2D sheet to anchoring organic/inorganic hybrid materials for the first time. The electrophoretically deposited film exhibited remarkably high photocurrent generation (IPCE = 70%) compared with the reference device without RGO sheets as well as ZnONP's. These results will provide a fundamental clue for the bottom-up construction of artificial photosynthetic systems utilizing organic/inorganic assemblies.

■ ASSOCIATED CONTENT

Supporting Information. Experimental details, and additional figures. This material is available free of charge via the Internet at http://pubs.acs.org.

■ AUTHOR INFORMATION

Corresponding Author
pkamat@nd.edu; imahori@scl.kyoto-u.ac.jp

■ ACKNOWLEDGMENT

This work was supported by a Grant-in-Aid (No. 21350100 to H.I.) and WPI Initiative, MEXT, Japan. H.H. is grateful for a JSPS Fellowship for Young Scientists. P.V.K. gratefully acknowledges the financial support of the Department of Energy, Office of Basic Energy Science. This is Contribution No. NDRL-4880 from the Notre-Dame Radiation Laboratory. We also thank Mr. Clifton Harris (Notre Dame Univ.) as well as Prof. Nicolai V. Tkachenko and Prof. Helge Lemmetyinen (Tampere Univ.) for the transient absorption spectra measurements.

■ REFERENCES

(1) *In Molecular Mechanism of Photosynthesis*; Blankenship, R. E., Ed.; Willey-Blackwell: Dordrecht, 2002.

(2) (a) Sun, L. C.; Hammarström, L.; Åkermark, B.; Styring, B. *Chem. Soc. Rev.* **2001**, *30*, 36. (b) Alstrum-Acevedo, J. H.; Brennaman, M. K.; Meyer, T. J. *Inorg. Chem.* **2005**, *44*, 6802. (c) Sheeney-Haj-Ichia, L.; Basnar, B.; Willner, I. *Angew. Chem., Int. Ed.* **2005**, *44*, 78. (d) Sisson, A. L.; Sakai, N.; Banerji, N.; Fürstenberg, A.; Vauthey, E.; Matile, S. *Angew. Chem., Int. Ed.* **2008**, *47*, 3727. (e) Imahori, H.; Umeyama, T. *J. Phys. Chem. C* **2009**, *113*, 9029. (f) Gust, D.; Moore, T. A.; Moore, A. L. *Acc. Chem. Res.* **2009**, *42*, 1890. (g) Wasielewski, M. R. *Acc. Chem. Res.* **2009**, *42*, 1910. (h) D'Souza, F.; Ito, O. *Chem. Commun.* **2009**, 4913. (i) Ardo, S.; Meyer, G. J. *Chem. Soc. Rev.* **2009**, *38*, 115. (j) Schulz-Drost, C.; Sgobba, V.; Gerhards, C.; Leubner, S.; Calderon, R. M. K.; Ruland, A.; Guldi, D. M. *Angew. Chem., Int. Ed.* **2010**, *49*, 6425. (k) Sagawa, T.; Yoshikawa, S.; Imahori, H. *J. Phys. Chem. Lett.* **2010**, *1*, 1020. (l) D'Souza, F.; Sandanayaka, A. S. D.; Ito, O. *J. Phys. Chem. Lett.* **2010**, *1*, 2586. (m) Sakai, N.; Bhosale, R.; Emery, D.; Mareda, J.; Matile, S. *J. Am. Chem. Soc.* **2010**, *132*, 6923. (n) Bhosale, R.; Misek, J.; Sakai, N.; Matile, S. *Chem. Soc. Rev.* **2010**, *39*, 138. (o) Kamat, P. V. *J. Phys. Chem. Lett.* **2011**, *2*, 242.

(3) Eu, S.; Hayashi, S.; Umeyama, T.; Matano, Y.; Araki, Y.; Imahori, H. *J. Phys. Chem. C* **2008**, *112*, 4396.

(4) Hummers, W. S.; Offeman, R. E. *J. Am. Chem. Soc.* **1958**, *80*, 1339.

(5) Lerf, A.; He, H.; Forster, M.; Klinowski, J. *J. Phys. Chem. B* **1998**, *102*, 4477.

(6) (a) Stankovich, S.; Dikin, D. A.; Piner, R. D.; Kohlhass, K. A.; Kleinhammes, A.; Jia, Y.; Wu, Y.; Nguyen, S. T.; Ruoff, R. S. *Carbon* **2007**, *45*, 1558. (b) Gómez-Navarro, C.; Weitz, R. T.; Bittner, A. M.; Scolari, M.; Mews, A.; Burghard, M.; Kern, K. *Nano Lett.* **2007**, *7*, 3499.

(7) Spanhel, L.; Anderson, M. A. *J. Am. Chem. Soc.* **1991**, *113*, 2826.

(8) (a) Williams, G.; Seger, B.; Kamat, P. V. *ACS Nano* **2008**, *2*, 1487. (b) Williams, G.; Kamat, P. V. *Langmuir* **2009**, *25*, 13869.

(9) Ng, Y. H.; Lightcap, I. V.; Goodwin, K.; Matsumura, M.; Kamat., P. V. *J. Phys. Chem. Lett.* **2010**, *1*, 2222.

(10) Umeyama, T.; Tezuka, N.; Fujita, M.; Hayashi, S.; Kadota, N.; Matano, Y.; Imahori, H. *Chem.—Eur. J.* **2008**, *14*, 4875.

(11) (a) Imahori, H.; Liu, J.-C.; Hotta, H.; Kira, A.; Umeyama, T.; Matano, Y.; Li, G.; Ye, S.; Isosomppi, M.; Tkachenko, N. V.; Lemmetyinen, H. *J. Phys. Chem. B* **2005**, *109*, 18465. (b) Imahori, H. *J. Mater. Chem.* **2007**, *17*, 31. (c) Kira, A.; Umeyama, T.; Matano, Y.; Yoshida, K.; Isoda, S.; Park, J. K.; Kim, D.; Imahori, H. *J. Am. Chem. Soc.* **2009**, *131*, 3198.

(12) (a) Kongkanand, A.; Kamat, P. V. *ACS Nano* **2007**, *1*, 13. (b) Brown, P.; Takechi, K.; Kamat, P. V. *J. Phys. Chem. C* **2008**, *112*, 4776.

(13) Lightcap, I. V.; Kosel, T. H.; Kamat, P. V. *Nano Lett.* **2010**, *10*, 577.

(14) Wojcik, A.; Kamat, P. V. *ACS Nano* **2010**, *4*, 6697.

(15) Czerw, R.; Foley, B.; Tekleab, D.; Rubio, A.; Ajayan, P. M.; Carroll, D. L. *Phys. Rev. B* **2002**, *66*, 033408.

(16) Subramanian, V.; Wolf, E. E.; Kamat, P. V. *J. Phys. Chem. B* **2003**, *107*, 7479.

(17) We performed transient absorption measurements for the FTO/SnO_2/(RGO+ZnONP+ZnP)$_m$ and FTO/SnO_2/(ZnONP+ZnP)$_m$ electrodes using the femtosecond pump−probe method with an excitation wavelength of 415 nm. However, formation of the charge-separated state in the mixed films could be detected because of a poor signal-to-noise ratio and the instability of the samples under the experimental conditions.